From laser ultrasonics to optical manipulation

Tomaž Požar,[*] Aleš Babnik, and Janez Možina

Faculty of Mechanical Engineering, University of Ljubljana, Aškerčeva 6, SI-1000 Ljubljana, Slovenia
[*]tomaz.pozar@fs.uni-lj.si

Abstract: During the interaction of a laser pulse with the surface of a solid object, the object always gains momentum. The delivered force impulse is manifested as propulsion. Initially, the motion of the object is composed of elastic waves that carry and redistribute the acquired momentum as they propagate and reflect within the solid. Even though only ablation- and light-pressure-induced mechanical waves are involved in propulsion, they are always accompanied by the ubiquitous thermoelastic waves. This paper describes 1D elastodynamics of pulsed optical manipulation and presents two diametrical experimental observations of elastic waves generated in the confined ablation and in the radiation pressure regime.

©2015 Optical Society of America

OCIS codes: (120.3180) Interferometry; (260.2160) Energy transfer; (280.3375) Laser induced ultrasonics; (320.5550) Pulses; (350.4855) Optical tweezers or optical manipulation.

References and links

1. J. Možina and R. Hrovatin, "Optodynamics - A synthesis of optoacoustics and laser processing," Prog. Nat. Sci. **6**, S709–S714 (1996).
2. J. Možina and J. Diaci, "Recent advances in optodynamics," Appl. Phys. B.-Lasers O. **105**(3), 557–563 (2011).
3. J. Možina and J. Diaci, "Optodynamics: dynamic aspects of laser beam-surface interaction," Phys. Scr. **2012**(T149), 014077 (2012).
4. C. B. Scruby and L. E. Drain, *Laser Ultrasonics: Techniques and Applications* (A. Hilger, 1990).
5. D. G. Grier, "A revolution in optical manipulation," Nature **424**(6950), 810–816 (2003).
6. R. M. White, "Generation of Elastic Waves by Transient Surface Heating," J. Appl. Phys. **34**(12), 3559–3567 (1963).
7. J. D. Aussel, A. Lebrun, and J. C. Baboux, "Generating acoustic waves by laser: theoretical and experimental study of the emission source," Ultrasonics **26**(5), 245–255 (1988).
8. S. Fassbender, B. Hoffmann, and W. Arnold, "Efficient Generation of Acoustic Pressure Waves by Short Laser-Pulses," Mater. Sci. Eng. A **122**(1), 37–41 (1989).
9. S. J. Davies, C. Edwards, G. S. Taylor, and S. B. Palmer, "Laser-Generated Ultrasound - Its Properties, Mechanisms and Multifarious Applications," J. Phys. D Appl. Phys. **26**(3), 329–348 (1993).
10. D. Royer and E. Dieulesaint, *Elastic Waves in Solids II: Generation, Acousto-optic Interaction, Applications* (Springer-Verlag, 2000), pp. 201–255.
11. C. Phipps, M. Birkan, W. Bohn, H. A. Eckel, H. Horisawa, T. Lippert, M. Michaelis, Y. Rezunkov, A. Sasoh, W. Schall, S. Scharring, and J. Sinko, "Review: Laser-Ablation Propulsion," J. Propul. Power **26**(4), 609–637 (2010).
12. Y. K. Bae, "Prospective of Photon Propulsion for Interstellar Flight," Phys. Procedia. **38**, 253–279 (2012).
13. N. Jain, "Laser Ultrasonics - The Next Big Nondestructive Inspection Technology?" Frost & Sullivan Market Insight (16. May 2011).
14. M. Mansuripur, "Momentum exchange effect," Nat. Photonics **7**(10), 765–766 (2013).
15. A. Schliesser, P. Del'Haye, N. Nooshi, K. J. Vahala, and T. J. Kippenberg, "Radiation pressure cooling of a micromechanical oscillator using dynamical backaction," Phys. Rev. Lett. **97**(24), 243905 (2006).
16. J. Možina and J. Diaci, "On-line Optodynamic Monitoring of Laser Materials Processing," in *Advanced Knowledge Application in Practice*, I. Fuerstner, ed. (InTech, 2010), pp. 37–60.
17. T. Požar, R. Petkovšek, and J. Možina, "Dispersion of an optodynamic wave during its multiple transitions in a rod," Appl. Phys. Lett. **92**(23), 234101 (2008).
18. T. Požar and J. Možina, "Homodyne Quadrature Laser Interferometer Applied for the Studies of Optodynamic Wave Propagation in a Rod," Stroj. Vestn.-J. Mech. E. **55**(10), 575–580 (2009).
19. T. Požar, P. Gregorčič, and J. Možina, "Optical measurements of the laser-inducedultrasonic waves on moving objects," Opt. Express **17**(25), 22906–22911 (2009).
20. T. Požar and J. Možina, "Optodynamic description of a linear momentum transfer from a laser induced ultrasonic wave to a rod," Appl. Phys. Adv. Mater. **91**(2), 315–318 (2008).
21. D. A. Hutchins, F. Nadeau, and P. Cielo, "A Pulsed Photoacoustic Investigation of Ultrasonic Mode Conversion," Can. J. Phys. **64**(9), 1334–1340 (1986).
22. J. P. Monchalin and J. D. Aussel, "Ultrasonic velocity and attenuation determination by laser-ultrasonics," J. Nondest. Eval. **9**(4), 211–221 (1990).

23. T. Požar and J. Možina, "Measurement of Elastic Waves Induced by the Reflection of Light," Phys. Rev. Lett. **111**(18), 185501 (2013).
24. J. C. Bushnell and D. J. McCloskey, "Thermoelastic Stress Production in Solids," J. Appl. Phys. **39**(12), 5541–5546 (1968).
25. N. Arnold, "Dry laser cleaning of particles by nanosecond pulses: Theory," in *Laser Cleaning*, B. Luk'yanchuk, ed. (World Scientific, 2002), pp. 51–102.
26. A. N. Pirri, "Theory for Momentum-Transfer to a Surface with a High-Power Laser," Phys. Fluids **16**(9), 1435–1440 (1973).
27. C. R. Phipps, T. P. Turner, R. F. Harrison, G. W. York, W. Z. Osborne, G. K. Anderson, X. F. Corlis, L. C. Haynes, H. S. Steele, K. C. Spicochi, and T. R. King, "Impulse Coupling to Targets in Vacuum by KrF, HF, and CO2 Single-Pulse Lasers," J. Appl. Phys. **64**(3), 1083–1096 (1988).
28. R. Fabbro, J. Fournier, P. Ballard, D. Devaux, and J. Virmont, "Physical Study of Laser-Produced Plasma in Confined Geometry," J. Appl. Phys. **68**(2), 775–784 (1990).
29. C. R. Phipps and M. M. Michaelis, "LISP: Laser impulse space propulsion," Laser Part. Beams **12**(1), 23–54 (1994).
30. T. Požar and J. Možina, "Mechanical wave motion due to the radiation pressure on gain or absorptive rods," Opt. Lett. **38**(10), 1754–1756 (2013).
31. A. A. Freschi, R. Hessel, M. Yoshida, and D. L. Chinaglia, "Compression waves and kinetic energy losses in collisions between balls and rods of different lengths," Am. J. Phys. **82**(4), 280–286 (2014).
32. M. Zhou, Y. K. Zhang, and L. Cai, "Adhesion measurement of thin films by a modified laser spallation technique: theoretical analysis and experimental investigation," Appl. Phys. Adv. Mater. **74**(4), 475–480 (2002).
33. K. Anju, K. Sawada, A. Sasoh, K. Mori, and E. Zaretsky, "Time-resolved measurements of impulse generation in pulsed laser-ablative propulsion," J. Propul. Power **24**(2), 322–329 (2008).
34. T. Požar, P. Gregorčič, and J. Možina, "A precise and wide-dynamic-range displacement-measuring homodyne quadrature laser interferometer," Appl. Phys. B-Lasers O. **105**(3), 575–582 (2011).
35. G. C. McLaskey and S. D. Glaser, "Acoustic Emission Sensor Calibration for Absolute Source Measurements," J. Nondestruct. Eval. **31**(2), 157–168 (2012).
36. M. Schneider, L. Berthe, R. Fabbro, and M. Muller, "Measurement of laser absorptivity for operating parameters characteristic of laser drilling regime," J. Phys. D Appl. Phys. **41**(15), 155502 (2008).
37. T. Požar, R. Petkovšek, and J. Možina, "Formation of linear momentum in a rod during a laser pulse-matter interaction," Appl. Phys. Adv. Mater. **92**(4), 891–895 (2008).
38. S. A. Akhmanov and V. É. Gusev, "Laser excitation of ultrashort acoustic pulses: New possibilities in solid-state spectroscopy, diagnostics of fast processes, and nonlinear acoustics," Sov. Phys. Usp. **35**(3), 153–191 (1992).
39. Optical Properties of Selected Elements," in *CRC Handbook of Chemistry and Physics*, 89th ed., David R. L., ed., (CRC Press/Taylor and Francis, 2009).
40. G. C. McLaskey and S. D. Glaser, "Hertzian impact: Experimental study of the force pulse and resulting stress waves," J. Acoust. Soc. Am. **128**(3), 1087–1096 (2010).
41. T. Požar, P. Gregorčič, and J. Možina, "Interferometric determination of the high-intensity laser-pulse-material interaction site," Appl. Phys. Adv. Mater. **112**(1), 165–171 (2013).
42. N. N. Hsu, "Dynamic Green's Functions of an Infinite Plate - A Computer Program," NBSIR 85–3234 (National Bureau of Standards, 1985), pp. 1–65.
43. P. N. Lebedev, "Untersuchungen über die Druckkräfte des Lichtes," Ann. Phys. (Berlin) **311**(11), 433–458 (1901).
44. E. F. Nichols and G. F. Hull, "A preliminary communication on the pressure of heat and light radiation," Phys. Rev. Ser. I **13**(5), 307–320 (1901).
45. J. H. Poynting, "On small longitudinal material waves accompanying light-waves," P. Roy. Soc. Lond. A. Mat. **85**(580), 474–476 (1911).
46. L. Voicu, L. Stamatescu, A. Hening, V. Raetchi, I. N. Mihailescu, and L. Nanu, "On the Signals Generated by Lead Zirconium Titanate (PZT) Ceramics when Irradiated with Microsecond Pulsed TEA-CO2 Laser Pulses," Phys. Status Solidi A **91**(2), K103–K106 (1985).
47. K. Kubota, "Optically-Excited Elastic Waves in Solids," Solid State Commun. **9**(23), 2045–2047 (1971).
48. M. Kobayashi, T. Miyachi, M. Hattori, S. Sugita, S. Takechi, and N. Okada, "Dust detector using piezoelectric lead zirconate titanate with current-to-voltage converting amplifier for functional advancement," Earth Planets Space **65**(3), 167–173 (2013).
49. T. Požar, "Oblique reflection of a laser pulse from a perfect elastic mirror," Opt. Lett. **39**(1), 48–51 (2014).
50. L. F. Bresse and D. A. Hutchins, "Transient generation of elastic waves in solids by a disk-shaped normal force source," J. Acoust. Soc. Am. **86**(2), 810–817 (1989).
51. M. Aspelmeyer, T. J. Kippenberg, and F. Marquard, "Cavity optomechanics," Rev. Mod. Phys. **86**(4), 1391–1452 (2014).

1. Introduction

Optodynamics, an application driven research field which investigates light-induced motion of macroscopic matter [1–3], strives to link together two, as we believe, inseparable fields of laser ultrasonics [4] and optical manipulation [5]. Laser ultrasonics concentrates in the laser generated elastic wave motion while optical manipulation investigates the means to move an object as a whole with no special interest in its internal relative motion. The ground for our

conviction lies in the physical picture which states that a macroscopic motion of a light-manipulated object is a superposition of its internal, time-developing wave motion.

When a reflective solid object is manipulated by a pulse of light, various types of elastic waves are launched from the illuminated surface towards the bulk of the solid [4,6–10]. In terms of decreasing amplitude, a high-intensity laser pulse gives rise to the following: *ablation-induced waves* (*AIWs*) resulting from material recoil, *thermoelastic waves* (*TEWs*) caused by light absorption and the subsequent thermal expansion, and the *light-pressure-induced waves* (*LIWs*) emanating exclusively from the photon linear momentum transfer. Even though the macroscopic motion of the object is the superposition of all these waves, as is schematically depicted in Fig. 1, only AIWs and the much weaker LIWs are involved in the translation of the object's center of mass. The former are the initial carriers of momentum in pulsed laser ablation propulsion [11] and the latter in pure-photon propulsion [12]. TEWs, on the other hand, are incapable of displacing an object, because, as a whole, they carry no linear momentum. Nevertheless, they are an indispensable tool in the nondestructive testing of materials [13].
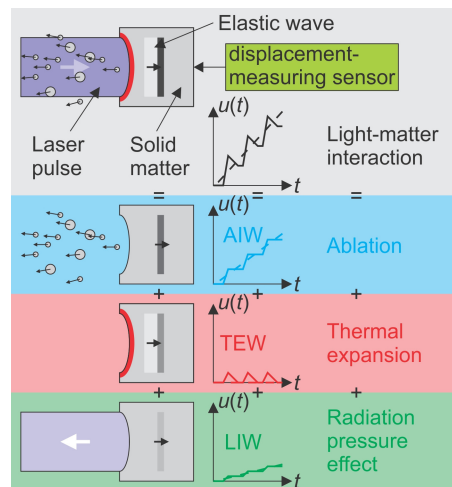

Fig. 1. Conceptual scheme of the elastic waves related to pulsed laser manipulation. Drawings on the left side on the figure recapitulate different light-matter interaction mechanisms. If the gray-code within the wave is paler that the undisturbed material, the wave is a rarefaction, and if it is darker, the wave is a compression. The graphs in the middle of the figure show the corresponding normal displacement of a rear surface of an 1D layer that can be detected with a suitable displacement-measuring sensor. The dashed line represents the displacement of the center of mass.

There is however a fundamental difference in the optodynamic mechanisms that govern the production of AIWs or LIWs. LIWs have its origin in radiation pressure which is inseparably connected with the linear momentum of electromagnetic waves or photons and its transfer during reflection or absorption, while AIWs are induced as a compensation for the momentum of the material expelled from the (near-)surface. The production of LIWs is thus a momentum related process while the birth of AIWs is a consequence of energy transformations.

So far, the macroscopic transfer of linear momentum to the solid due to various types of light-matter interactions has been inferred predominantly by observing the motion of the center of mass of the manipulated object. Nowadays, this exchange of momentum is found in many applications. In the micro world, it is used, for example, to manipulate small objects (laser tweezers) [5,14] and for material cooling (laser cooling) [15]. In the macro world, such transfer of momentum finds applications all the way from laser material processing [16] to laser-propulsion schemes [11].

In this paper, we concentrate our interest on the elastodynamic nature of the momentum transfer in optical manipulation. By overcoming the constraint of inelastic, rigid-body motion of the light-manipulated object, we observe the true nature of propulsion that includes elastic waves. In pulsed laser propulsion, the acquired momentum is initially localized within the propagating AIWs and LIWs. As time passes, moderate effects of dispersion, internal damping, etc., gradually redistribute the momentum from within the initial mechanical waves to the final net motion of the whole solid. It is thus only later that a light-propelled elastic solid can be considered as carrying the momentum as a rigid body.

The reader, interested in mechanisms that redistribute the linear momentum from the initial mechanical wave to the final gross motion that has no relative particle motions, after the mechanical waves completely die away, should find the relevant information in the following literature. The effects of dispersion on the redistribution of momentum are presented in [17]. Those due to either localized or homogeneously distributed friction are given in [18] and [19], respectively. The leakage of momentum into the atmosphere surrounding the propelled object is shortly described in [20]. Other mechanisms include: mode conversion of elastic waves [21] and internal attenuation [22].

After a concise theoretical introduction, we will review and compare two unique measurements revealing AIWs and LIWs. First, an AIW with a very large amplitude of 650 nm was induced in the confined ablation regime at the front end of a rod [19]. A contactless displacement measurement of a laser-propelled rod's rear end was then performed with a homodyne quadrature laser interferometer during the entire duration of its motion. This is an experimental demonstration of a laser-propelled, elastic-body motion where all the significant physical mechanisms that reveal the nature of its motion are seen from a single-shot measurement.

In the second experiment, we elucidate the detection of LIWs [23], which are notoriously difficult to be resolved due to the presence of the dominating AIWs and TEWs. Initially, we show experimentally that TEWs can be sufficiently suppressed using an ultrahigh-reflectivity (HR) mirror so that LIWs become detectable. The LIW's reverberations, causing merely few picometer-large displacement-steps of the mirror's rear facet, were observed with a calibrated piezoelectric sensor.

2. Theory

The goal of this section is to explain the 1D elastic motion of a solid object that is propelled by a laser pulse. First, we will discuss different regimes of sources that generate elastic waves and then their propagation within the solid.

Consider a cross section A of a 1D, quasi-monochromatic plane-wave laser pulse of energy $E_i = \int_0^{t_i} P_i(t)dt$, duration t_i, an arbitrary temporal distribution of power given by $P_i(t)$ and linear momentum $p_i = E_i/c$ impinging from free-space with velocity c, normal to the surface of homogeneous and isotropic, elastic infinite layer having a mass density ρ, thickness L and a longitudinal wave velocity c_P that has stress-free surfaces and is initially at rest. During the interaction of the laser pulse with the (near-)surface of an opaque solid, and also after the interaction in the case of ablation that is accompanied by an expanding plasma, the surface of the solid experiences a time-dependent pressure $\mathsf{P}(t)$ with duration t_e, whose integral is a pressure impulse that equals the linear momentum $\Delta p = A\int_0^{t_i < t_e} \mathsf{P}(t)dt$ transferred to the solid per unit surface area A.

This pressure pushes the front surface inward towards the bulk of the solid and displaces it by u_0. The quantity u_0 is called *the amplitude of the wave* and is intimately connected with the transferred momentum

$$\Delta p = m_0 c_P = \rho u_0 A c_P = Z A u_0 , \qquad (1)$$

which is localized within the $c_P t_e$-long propagating compression. Here, m_0 equals the mass of the moved volume $u_0 A$ and $Z = \rho c_P$ is the acoustic impedance of the solid. Similar arguments that lead to the same relation [Eq. (1)] can be found in [20]. The amplitude u_0 is interpreted as the total displacement experienced by any cross section within the layer after it is completely passed over by a transient elastic wave that carries the momentum Δp.

2.1 Light-pressure-induced waves (LIWs)

First, a separate evaluation of Δp will be made for LIWs that are generated exclusively by radiation pressure. The laser pulse carries p_i of momentum and at normal incidence ($\alpha = 0°$) the amount $\Delta p = (1 + R)E_i/c$ is transferred to the solid with surface power reflectivity R. The non-reflected fraction of the pulse energy $(1 - R)E_i$, when absorbed in an opaque solid, gives rise to TEWs. It follows from Eq. (1) that the amplitude of the LIWs is

$$u_0 = \frac{1+R}{Zc} q_i \,, \tag{2}$$

with $q_i = E_i/A$ being the fluence of the laser pulse. The radiation pressure experienced by the surface is $\mathsf{P}(t) = P_i(t)(1+R)/(cA) = I_i(t)(1+R)/c$ and $I_i(t) = P_i(t)/A$ is the time-dependent light intensity of the laser pulse.

A figure of merit relevant to laser propulsion is the momentum-coupling coefficient C_m, defined as the ratio of the transferred momentum Δp and incident optical energy E_i. It can also be expressed as the ratio between the pressure $\mathsf{P}(t)$ acting on the surface and the laser pulse intensity $I_i(t)$. The pure-photon momentum-coupling coefficient is

$$C_m = \frac{\Delta p}{E_i} = \frac{\mathsf{P}(t)}{I_i(t)} = \frac{1+R}{c} = \frac{Z}{q_i} u_0 \,. \tag{3}$$

It has a linear dependence on the amplitude of the wave. In the case of a perfect reflector ($R = 1$), it reaches its maximum theoretical value of 6.67 nNs/J.

2.2 Thermoelastic waves (TEWs)

Due to the physics behind their generation, TEWs carry no total linear momentum ($\Delta p = 0$), because they are always composed of compressions and rarefactions with balancing momenta. Since the transiently heated, mechanically free surface pushes on itself, there has to be an equal amount of forward pointing momentum within the compression and backward pointing momentum within a rarefaction. 1D mathematical model of TEWs generated due to laser pulse absorption within the penetration depth of a mechanically free surface and its instantaneous expansion predicts that the leading phase of a bi-polar longitudinal acoustic pulse is a compression followed by a rarefaction [24,25] with an amplitude of $u_0 = (1 - R)q_i\alpha/(2\rho C)$ [4,24], where C is the specific heat capacity and α is the coefficient of linear thermal expansion.

The TEWs have no ability to displace the center of mass of the object within which they propagate. In general, their amplitude is much larger than the amplitude of LIWs. Their amplitudes become equal when $1 - R = 4\kappa$ and $\kappa \approx C/(\alpha c_P c) \approx c_P/c$. For this condition to be fulfilled, a minute surface absorbance, often as small as 10^{-5}, is required. Thus, to discern LIWs from the dominating TEWs, a laser pulse should be reflected from a highly reflective surface with R exceeding 99.999%.

2.3 Ablation induced waves (AIWs)

In general, modelling of momentum transfer to the surface of the solid in the ablation regime is complicated [26–29]. Therefore, we will consider here only a simple model where $(1 - R)E_i$ of the incident laser energy is absorbed and used exclusively to evaporate a thin layer from the surface of the solid. The vapor is blasted from the surface and the reaction gives rise to a

pressure impulse pressing on the surface. The simplest assumption is that the absorbed optical energy is used to evaporate the target and deliver the needed kinetic energy to the expelled vapor and that intensity is below the threshold for plasma formation. Employing these assumptions, the transferred momentum is $\Delta p = mv_e = E_i v_e (1 - R)/L_B$, where m is the evaporated mass, v_e is the eject velocity of the vapor and L_B is the latent heat of vaporization. Inserting the above expression for the transferred momentum into Eq. (1) yields an AIW's amplitude of $u_0 = (1 - R)q_i v_e/(ZL_B)$.

The momentum-coupling coefficient equals

$$C_m = \frac{1-R}{L_B} v_e \qquad (4)$$

and is proportional to the eject velocity of the vapor, the absorbed optical energy and inversely proportional to the heat required to evaporate the material, while the pressure is

$$\mathsf{P}(t) = \frac{1-R}{L_B} v_e I_i(t). \qquad (5)$$

2.4 Elastic response of the propelled solid – 1D problem

Here, we summarize the main conclusions that can be drawn from the 1D analytical displacement field $u(x,t)$ derived in detail in [30]. Due to light-matter interaction, the front surface ($x = 0$) of the infinite solid layer ($0 < x < L$) experiences a time-dependent pressure given by $\mathsf{P}(t)$. The pressure enters the general boundary condition at the front surface $\left.\dfrac{\partial u(x,t)}{\partial x}\right|_{x=0} = -\dfrac{\mathsf{P}(t)}{\rho c_P^2} = -C_m \dfrac{I_i(t)}{\rho c_P^2}$. This condition supplements the 1D Euler-Bernoulli equation of elastodynamics. In the radiation pressure regime, $\mathsf{P}(t)$ is proportional to $I_i(t)$, but this is not necessarily the case in the ablation regime [28]. It is only true in the simple model given in Eq. (5). The factor of proportionality C_m thus depends on the propulsion regime and is given in Eqs. (3) and (4).

The displacement field, valid for $0 < t$, is expressed as the convolution of the impulse response—the Green's function $\Gamma(x,t)$—with the intensity profile $I_i(t)$

$$u(x,t) = \Gamma(x,t) * I_i(t) = \int_0^t \Gamma(x,\xi) I_i(t-\xi) d\xi. \qquad (6)$$

The Green's function Γ takes into account reverberations of the transient elastic wave within the free-free elastic layer of length L. It is composed of a series of Green's functions for an elastic half-space $G(x,t) = C_m \mathsf{H}(c_P t - x)/Z$ as

$$\Gamma(x,t) = \sum_{n=0}^{\infty} \left[G(x, c_P t - 2nL) + G(2L - x, c_P t - 2nL) \right], \qquad (7)$$

with H being the Heaviside step function.

If one takes a convenient intensity distribution, for example with a form

$$I_i(t) = q_i \frac{t}{t_0^2} e^{-t/t_0} \qquad (8)$$

that represents a pulse with a steep rise, FWHM of 2.4 t_0, and a more gently sloping tail, an analytical displacement field [Eq. (6)] is obtained by convolving Eqs. (7) and (8).

The displacement of the layer's center of mass $u^*(t)$ is obtained by integrating the corresponding velocity which is, again, the integral that involves the time-dependent intensity

$$u*(t) = \frac{C_\mathrm{m}}{Zt_L} \int_0^t \left[\int_0^{t'} I_\mathrm{i}(t'')\mathrm{d}t'' \right] \mathrm{d}t' . \tag{9}$$

To demonstrate the motion of the layer, consider an example where the propulsion mechanism is solely due to radiation pressure. Deliver a Q-switched laser pulse with a fluence of $q_\mathrm{i} = 1$ J/cm^2 normally onto the front surface of a perfect mirror ($R = 1$). The shape of a Q-switched pulse is well modeled by the distribution given in Eq. (8). A typical value for the FWHM is 10 ns which corresponds to $t_0 = 4.2$ ns. Take an ultrahigh-reflectivity-coated UV-grade fused silica layer with $\rho = 2200$ kg/m^3, $c_\mathrm{P} = 5931$ m/s and thickness $L = 6.35$ mm. The acoustic impedance is $Z = 13.0$ MRayl, the calculated amplitude of the LIW [Eq. (2)] is $u_0 = 5.08$ pm, the time-of-flight across the thickness of the layer is $t_L = L/c_\mathrm{P} = 1.06$ µs, and the delivered pressure impulse equals $C_\mathrm{m}q_\mathrm{i} = 66.7$ µPa·s. For the above given parameters (the black lines) and for a 50-times wider laser pulse (the gray lines), the theoretical motion of the layer's rear surface is presented in Fig. 2.
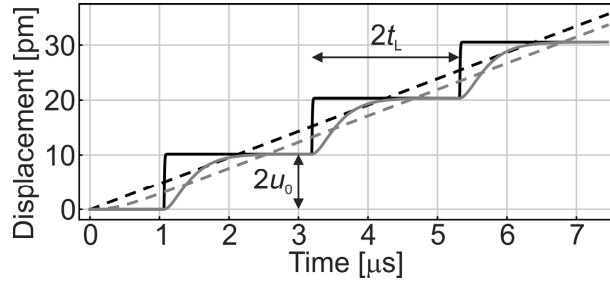

Fig. 2. Theoretical out-of-plane displacement of the rear surface of an infinite layer as a function of time. Dashed lines: the motion of the layer's center of mass $u*(t)$, Eq. (9). Solid lines: discrete staircase-like displacement $u(x = L,t)$, Eq. (6), caused by an elastic wave reverberating within the free-free layer. Black lines: FWHM = 10 ns or $t_0 = 4.2$ ns. Gray lines: FWHM = 0,5 µs.

The motion, depicted in Fig. 2, deserves additional explanation. The elastic wave is born at the front surface as a compressional wave, because forces press the front surface towards the bulk of the layer. When it arrives at the rear facet, it reflects backwards. During the reflection, the rear surface of the layer moves forward by $2u_0$ and remains there. Due to the impedance mismatch at the rear surface of the layer, the reflected mechanical wave switches from a compression to a rarefaction and travels back to the front surface where it exerts a pull on it, reflects again, turns into compression and propagates forward. Thus, the displacement of the rear side of the solid layer $u(x = L,t)$ resembles a staircase-like motion. Each time the elastic wave reflects from the rear side, discrete displacements of height $2u_0$ occur. This happens at times $(2n - 1)t_L$, $n = 1,2, \ldots$, after the first contact of the laser pulse with the front surface [31]. If the pressure impulse is shorter that the double time-of-flight ($t_\mathrm{e} < 2t_L$), then the shape of the step is proportional to the integral of the time-dependent pressure. Since a compression displaces any cross section that it transverses in the same direction as it propagates, the momentum within it points in the direction of propagation. On the contrary, a rarefaction pulls on the material that is passes over and, consequently, its momentum points in the direction opposite to the propagation.

Staircase-like motion of the free surface has also been observed during laser-spallation process of transparent thin films deposited on opaque substrates [32] and in time-resolved measurements of pulsed laser-ablative propulsion [33]. When all the experiments with laser-induced staircase-like motion are compared, the following common characteristics can be identified. A reverberating, longitudinal, mono-polar mechanical pulse is generated within the solid propagating perpendicularly to solid's plan-parallel free surfaces and the employed displacement-measuring technique features high temporal resolution. In order to distinguish the discrete steps, the length on the mono-polar wave is shorter than twice the thickness on the solid.

Table 1. Experimental parameters and measured/calculated values

	AIWs [19]	LIWs [23]
Detector	**Homodyne quadrature laser interferometer (HQLI) [34]**	**Conical piezoelectric sensor (PZT) [35]**
Bandwidth	flat: DC – 200 MHz	nearly flat: 50 kHz – 2.5 MHz
Noise floor (single shot)	0.1 nm	< 1 pm
Dynamic range	$\sim 10^6$	$\sim 10^3$
Averaging	Single shot	$\times$ 50 (repetition 1 Hz)
Material of the propelled object	**Steel (AISI: 304) – (rod)**	**Ultrahigh-reflectivity-coated UV-grade fused silica – (slab)**
Surface power reflectivity R	$\sim 65\%$ [36]	> 99.999%
Mass density ρ [kg/m^3]	7900	2200
Thin-rod velocity c_0 [m/s]	5100	/
Longitudinal wave velocity c_P [m/s]	/	5931
Acoustic impedance Z [MRayl]	40.3	13.0
Length L [mm]	120	6.35
Diameter [mm]	2.0	25.4
Time-of-flight [μs]	23.5	1.07
Laser source	**Q-switched Nd-YAG**	**Q-switched Nd-YAG**
Mode	Multimode	Top-hat
Wavelength λ_i [nm]	1064	1064
Max. energy per pulse [J]	0.3	1.6
FWHM pulse duration [ns]	10	10
Experimental fluence [J/cm^2]	$\sim 4 \times 10^3$	< 2
Exp. intensity I_i [W/cm^2]	$\sim 4 \times 10^{11}$	$< 2 \times 10^8$
Interaction regime	**Confined ablation**	**Pure-photon**
Front surface	Covered with a water droplet	HR coating R > 99.999%
Amplitude of the wave u_0 [nm]	650	< 0.020
Transferred momentum Δp [Ns]	82×10^{-6}	3.3×10^{-9}
Momentum-coup. coeff. C_m [Ns/J]	3×10^{-4}	6.67×10^{-9}

3. Measurements

We will review two diametrical measurements of elastic waves generated with laser pulses. The first one was made in the confined ablation regime producing AIW with a large amplitude of 650 nm [19] and the second one was performed exclusively by radiation pressure, yielding minute LIWs with 5-orders-of-magnitude smaller amplitudes [23]. The details of both experiments are compared side-by-side in Table 1. Additionally, we experimentally demonstrated how to suppress TEWs so that LIWs can be discerned in the detected waveforms.

3.1 Detection of ablation-induced waves (AIWs)

Figure 3(a) shows the experimental setup where the rear-end displacement $u(x = L,t)$ of the cylindrical sample (rod) is measured with a homodyne quadrature laser interferometer (HQLI) after the front facet of the rod was ablated with a single-shot, focused, multimode, Q-switched Nd:YAG (WallBlaster, Fotona, Slovenia) laser pulse with E_i = 300 mJ. The theoretical [Fig. 3(d)] and measured [Figs. 3(b) and 3(c)] staircase-like axial displacements of the rear surface of a 120-mm long steel rod with a diameter of 2 mm and water covered front facet are also shown.

The displacement in Fig. 3(d) was modelled using an analytical solution of Love's equation for a free-free homogeneous rod which, additionally to the staircase-like motion, includes the effects or lateral inertia [17]. The dispersion effects due to lateral inertia, not comprised in Eq. (6), are visible as high-frequency oscillations superimposed on the larger, discrete displacement steps and are present in Figs. 3(c) and 3(d). The large discrete steps are described by Eq. (6) if c_P is replaced by a thin-rod velocity c_0.
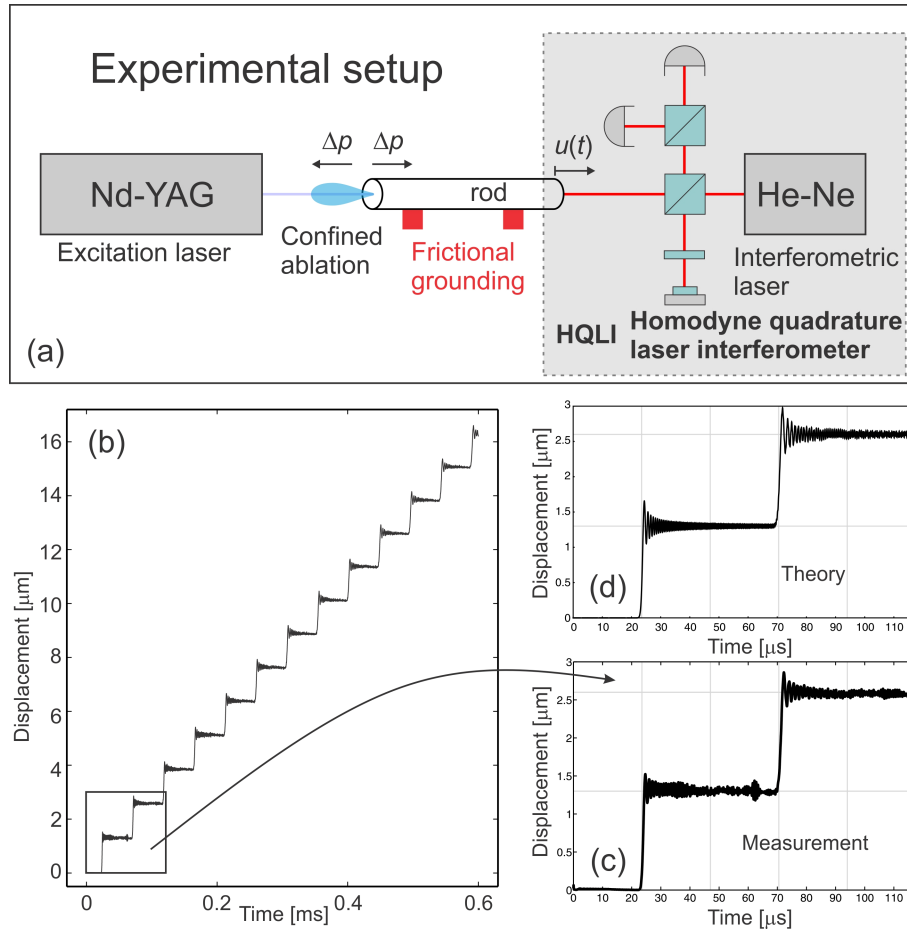
Fig. 3. Detection of AIWs. (a) Experimental setup. (b),(c) Measured rear-end displacement of the rod in the first 600 μs (b) and 120 μs (c). (d) Theoretical displacement corresponding to inset (c).

When the transiently propelled rod is considered to be a rigid body or when its motion is measured with a low-resolution technique, the rear-facet displacement follows a straight line if deceleration arising from the frictional forces between the rod and the grounding in contact is negligible. A high-resolution HQLI was employed to demonstrate the richness of the nature of elastic-body motion that reveals the staircase-like motion which is clearly visible in Fig. 3(b). Here, the motion immediately after the laser pulse is restricted to the mechanical wave as described by Eq. (6). This wave is much shorter compared to the length of the rod L. Thus, Fig. 3(b) implies that the mechanical wave, which is concealed in the elastic body, is responsible for its motion. The motion takes place only within the mechanical wave, while the other parts of the rod are at rest if high-frequency oscillations are neglected.

The measured AIW's amplitude $u_0 = 650$ nm (half of the step's height) was used to scale the theoretical curve in Fig. 3(d) and to determine the transferred momentum during the laser-material interaction and the momentum-coupling coefficient (see Table 1). In comparison with the ballistic methods, these values were obtained on a two orders of magnitude shorter time scale [37].

3.2 Suppression of thermoelastic waves (TEWs)

LIWs are notoriously difficult to detect, because the measured waveform is usually dominated by the simultaneous emission of TEWs [6,23,38]. As has already been mentioned,

the reflection of light gives rise to a LIW with an amplitude which is comparable to the amplitude of the TEW when about 10^{-5} of the incident laser pulse energy is absorbed near the illuminated surface [30]. This, and experimentalists' frequent usage of reflective metals with $R \ll 99.999\%$, is the main reason why, until recently [23], LIWs were hidden from detection. Thus, it will be presented how to reduce the generation of TEWs in order to discern the presence of LIWs.
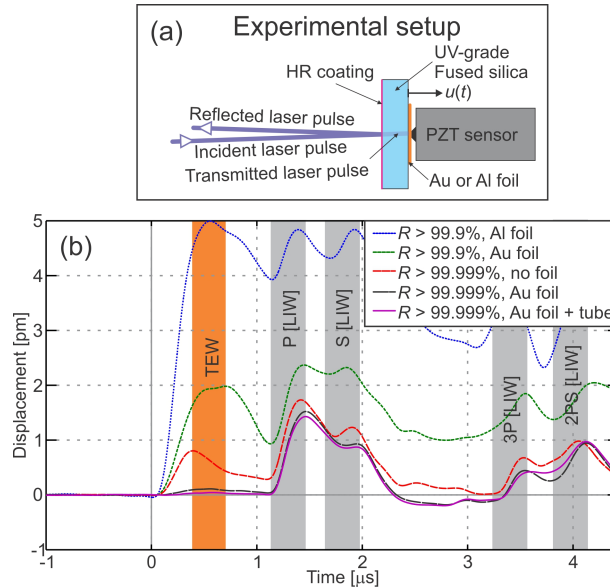

Fig. 4. Suppression sequence of TEWs. (a) Experimental setup. (b) Measured rear-surface out-of-plane displacement of the mirror in the first 4.41 µs. TEW peak is detected at 0,5 µs. LIW components' arrival times: P at 1.07 µs, S at 1.70 µs, 3P at 3.21 µs and 2PS at 3.84 µs.

Experimental demonstration of the TEW suppression sequence is presented in Fig. 4. The setup, schematically shown in Fig. 4(a), employs a Q-switched Nd:YAG laser (Brio, Quantel, France). It emits 4 ns (FWHM) pulses with energy of 60 mJ and wavelength of 1064 nm. Since the light pulse, impinging by a small angle (~1°) on the center of the dielectric HR coating applied on a UV-grade fused silica substrate, illuminates a circular area with a radius smaller that the thickness of the mirror, the geometry is no longer one-dimensional. Therefore, the 1D theoretical curves presented in Fig. 2 no longer apply.

Two mirrors with the same dimensions (diameter d = 25.4 mm and thickness L = 6.35 mm) were used. The least reflective one has a HR coating with a nominal reflectivity $R >$ 99.9% (L-00612, Laseroptik, Germany), while the ultrahigh-reflectivity mirror features $R >$ 99.999% (HRM01-1064RINF-25.4, ATFilms, USA). Elastic waves were detected with a calibrated, displacement-measuring, conical piezoelectric (PZT) sensor (KRNBB-PC, KRN Services, USA) [35] that was brought in contact with the center of the rear facet of the mirror. It has a nearly flat sensitivity in the frequency range from 50 kHz to 2.5 MHz and a single-shot noise floor smaller than 1 pm.

Five different out-of-plane displacement waveforms are presented in the first 4.41 µs after light reflection [Fig. 4(b)]. To enhance the signal-to-noise ratio, each waveform was averaged over 200 repeatable events with a 0.645-Hz repetition rate. Waveforms were additionally smoothed by a 2nd-order low-pass digital Butterworth filter with a cutoff frequency of 5 MHz. The two with the largest amplitudes were obtained with the $R >$ 99.9% mirror while the other three were measured on an $R >$ 99.999% mirror. Since the contact plate of the PZT sensors is made of nickel (R = 73% at 1064 nm [36,39]) with a relatively small reflectivity, golden (R = 99% at 1064 nm [36,39], thickness: 20 µm) or aluminum (R = 96% at 1064 nm

[39], thickness: 10 μm) foils were sandwiched between the sensor and the rear facet of the mirror in order to further decrease the absorption of the laser pulse by the PZT sensor.

Had no light reached the sensor, heating would not have taken place and therefore no TEW was generated at the tip of the PZT cone. In this case, no motion should be detected until the fastest propagating P-component of the LIW with its origin in the epicentral position is expected to arrive at the rear facet on the other side of the mirror at $t_P = L/c_P = 1.07$ μs, where $c_P = 5931$ m/s is the velocity of propagation of the bulk longitudinal elastic disturbance. Due to a 2D geometry, the P-component is accompanied by a slower propagating shear S-component of the LIW which arrives at $t_S = L/c_S = 1.70$ μs, where $c_S = 3740$ m/s. The first echo of the LIW's P-component arrives at $t_{3P} = 3L/c_P = 3.21$ μs. Another arrival, the mode converted LIW's 2PS-component, is detected at 3.84 μs before the reflection of the P-component from the side walls at about 4.41 μs ruins the infinite plate geometry. Except for the presence of the initial TEW, the general shape of the detected waveforms has all the relevant features as the epicentral waveforms obtained with other detectors and other normal-force sources, such as: ball-impact [40] and laser-ablation [41]. Normal displacement of the surface caused by the arrivals of P-, S-, 3P-, and 2PS-components are also predicted by the epicentral theoretical solutions [42]. When the sensor is placed directly beneath the source, the detected waveforms are insensitive to small changes in the source or sensor locations [35].

The waveform with the largest TEW was obtained when Al foil was placed between the sensor and the $R > 99.9\%$ mirror. In this case, about 4×10^{-5} of the incident laser pulse energy was absorbed in the aluminum foil. Localized thermal expansion gave rise to a TEW, whose peak is seen at 0.5 μs. When Al foil was replaced by an Au foil, less energy (now only about 1×10^{-5}) was absorbed in the foil and the TEW peak was reduced from 5 pm to 2 pm. Employing an ultrahigh-reflectivity mirror and using no shielding foil, about 0.3×10^{-5} of the incident energy is absorbed directly on the nickel faceplate of the PZT sensor. The peak of the TEW was further reduced to 0.8 pm. Inserting an Au foil, the absorbed energy falls to 0.01×10^{-5} and the TEW peak's amplitude of 0.11 pm becomes barely detectable. The presented detection scheme is so sensitive, that further reduction of the TEW was possible when Rayleigh scattered light of the incident pulse in the air was partially blocked by delivering the pulse through a tube. Here, the peak of the TEW was merely 40 fm compared to the 1.4-pm-large peak of the LIW's P-component.

3.3 Detection of light-pressure-induced waves (LIWs)

Soon after the first experimental verification of radiation pressure at the turn of the century from Lebedev [43] and, independently, from Nichols and Hull [44], Poynting [45] foretold the existence of "*small longitudinal material waves accompanying light-waves*". It is only later that LIWs drew attention again, this time with the advent of laser ultrasonics [6]. But it was soon found that their amplitudes are significantly smaller than the accompanying TEWs, because experiments were mainly performed on reflective metals. Again, the interest for LIWs ceased.

It is, however, worth noting that experimental attempts falsely claiming detection of LIWs do exist [38]. One such excursion is described in the paper by Voicu et al. [46]. Since their experiments were performed on Al with the reported R of 97.5% at 10.6 μm, we have strong reasons to believe that the dominating waveforms were due to thermoelastic expansion rather than merely caused by radiation pressure. Similar assertions were also given by Kubota for elastic wave generation in various opaque materials [47] and Kobayashi et al. for laser pulse reflection from a silver electrode on a PZT cube [48]
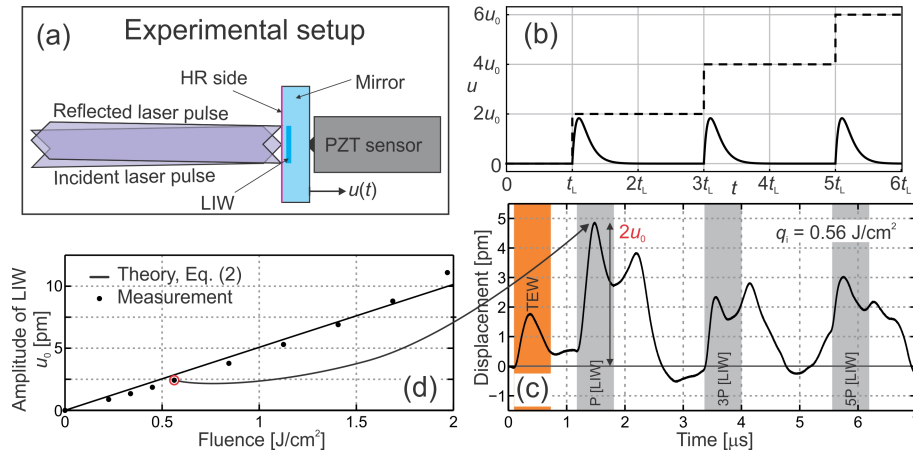
Fig. 5. Detection of LIWs. (a) Experimental setup. (b) Theoretical displacement of the rear side of the mirror. Dashed black line: discrete staircase-like motion. Solid black line: the simplified expected waveform considering the clamping of the mirror and the transfer function of the PZT sensor. (c) Measured rear-surface displacement of the mirror in the first 7 μs for $q_i = 0.56$ J/cm². (d) Comparison between the measured LIW amplitudes (dots) and the theory [solid line, Eq. (2)]

The feasibility of TEW suppression lead us to assemble an experimental system, shown in Fig. 5(a), which enables the detection LIW's amplitude that conforms to the theoretical value given by Eq. (2). Unfocused top-hat laser pulses (QX MAX, Fotona, Slovenia), are incident at an angle $\alpha = 1°$, to prevent laser-pulse reentry into the cavity, and illuminate a circular area with an 8-mm diameter at the center of the clamped mirror. This small angle enters Eq. (2) as a multiplicative factor $\cos^2\alpha$ [49] that equals 0.9997 and can be neglected when $\alpha = 1°$. The same conical PZT element is brought into contact with the rear side of the mirror in its center without the use of the shielding Au/Al foil. Because of the transfer function of the PZT sensor and its tip in contact with the measuring surface, the expected waveform that indicates LIW rear surface reflections differs from the staircase-like motion (Fig. 2) as shown in Fig. 5(b).

Figure 5(c) presents the measured waveform in the first 7 μs after the laser-pulse recoil, averaged over a train of 50 consecutive 0.56 J/cm² pulses. The first three reverberations (P, 3P and 5P) of the LIW's P-component are clearly distinguishable in Fig. 5(c) for their expected arrival times. The measured amplitude u_0 of the LIW is taken from the peak ($2u_0$) of the first P arrival when the geometry can still be regarded as one dimensional. This waveform is similar to the waveform ($R > 99.999\%$, no foil) in Fig. 4(b). However, the peak of the LIW's S-component is more pronounced due to the waves emitted from the edge of the disk-shaped normal force source [50].

The comparison between the theoretical LIW's amplitude, as given by Eq. (2), and the LIW's amplitude measured at different fluences is shown in Fig. 5(d). The theory and measured points closely match up to the fluence of 2 J/cm². Above this value, the laser-induced damage threshold of the mirror is surpassed and the ultrahigh-reflectivity coating becomes permanently damaged.

By first impression, the experimental system shown in Fig. 5(a) reminds us of the experiments performed in the contemporary research field of cavity optomechanics [51]. Since we are using a single mirror, instead of two, which is needed to form an optical cavity, we have no circulating light. The coupling of the light-mirror system is much simpler in our case compared to cavities, where the cavity resonantly enhances the circulating intensity and thus makes it depend very sensitively on the position of the mirrors.

The presented measurements of LIWs provide the first quantitative, direct evidence of light-pressure-induced elastic waves (LIWs) in solids. These waves are generated solely by the momentum transfer from the light to an elastic solid and are the most basic fingerprint of a light-solid matter interaction on the macroscopic scale.

4. Conclusions

The treatment of optical manipulation or laser propulsion of solid objects inevitably leads to the wrong physical conclusions if the object is considered simply as a rigid body. The most significant consequence of this unphysical picture is the transfer of information from the illuminated side to the opposite one with infinite velocity. This paper revealed a more detailed understanding of optical manipulation that is consistent with the principles of causality and agrees with experimental observations obtained in two distinct interaction regimes: confined ablation and pure radiation pressure. It also bridges the research areas of laser ultrasonics and optical manipulation.

Even though most of the presented material was limited to 1D geometry, the elastodynamic description of laser propulsion of solid objects in terms of the superposition of the ablation-induced waves (AIWs), the thermoelastic waves (TEWs) and the light-pressure-induced waves (LIWs) remains similar also in three dimensions. Likewise, the constraint of short pulsed light can be extended to CW propulsion/manipulation regime without loss of generality.

The measured waveform clearly demonstrated the staircase-like discrete motion of the rod's rear surface when the interaction took place in the confined ablation regime. The AIW's large amplitude of 650 nm permitted the observation of the rod's motion with a wide-bandwidth interferometer. On the other hand, a more sensitive conical PZT sensor had to be deployed on the rear surface of the ultrahigh-reflectivity mirror to discern the minute, few picometers large LIWs. The suppression of TEW's amplitude below 20 fm enabled the first, isolated detection of LIWs with a 35-times larger amplitude. Based on this experimental research, light pressure effects on solid matter can now be inferred by the detection of LIWs.

A superposition of laser-induced elastic waves is not only an orderly treatment of pulsed optical manipulation. It also provides the platform for the determination of propulsion-relevant parameters, such as, the transferred momentum during the laser-material interaction and the momentum-coupling coefficient.